J Solid State Electrochem (1998) 2: 285–290

ORIGINAL PAPER

C. Lenain · L. Aymard · J.-M. Tarascon

Electrochemical properties of Mg_2Ni and Mg_2Ni_2 prepared by mechanical alloying

Received: 8 October 1997 / Accepted: 20 January 1998

Abstract Crystallized Mg_2Ni and Mg_2Ni_2 amorphous alloys synthesized by mechanical alloying at room temperature were found to present first discharge capacities of 270 mAh/g and 500 mAh/g, respectively. These capacities decrease upon subsequent cycling to reach 30 mAh/g and 70 mAh/g after 60 charge/discharge cycles. The largest initial capacity, measured for the Mg_2Ni_2 composition, is ascribed to its amorphous nature, while its poor capacity retention upon cyding appears to originate from a fine Ni dispersion within the Mg/Ni matrix. This dispersion enables a better protection of the Mg against oxidation during cycling. We show, however, that this protection of Mg by Ni is not sufficient to avoid a strong corrosion of Mg in the KOH electrolyte during cycling, leading to the formation of $Mg(OH)_2$.

Key words Mg-Ni alloys · Mechanical alloying

Introduction

Soon after the discovery in the late sixties that intermetallic compounds such as $LaNi_5$ were able to absorb/desorb large amounts of hydrogen gas, it was realized that hydride-forming materials could serve as a new energy storage medium. Thirty years later, nickel-metal hydride (NiMeH) batteries based on hydride-forming electrodes are widely used in the portable consumer electronic market, mainly replacing the Ni-Cd batteries. The NiMeH battery technology presents advantages over the Ni-Cd battery technology both in terms of environmental issues, since it does not use toxic chemical elements such as Cd, and in terms of gravimetric capacity, which can exceed that of Ni-Cd by at least 25%.

C. Lenain · L. Aymard · J.-M. Tarascon (✉)
Université de Picardie Jules Verne, LRCS, 100 rue Saint Leu, F-80039 Amiens, France

Two types of metallic alloys are presently used in commercial NiMeH for portable electronics. They are the AB_5 class of alloys (A = Mischmetall, B = Ni, Co, Al, Mn, Si) [1–3], and the AB_2 class of alloys (A = Ti, Zr, B = Ni, V, Cr...) [4–12]. However, for targeting the field of vehicular propulsion with NiMeH technology, better hydrogen-absorbing alloys than AB_5 or AB_2 types in terms of higher energy density and cycle life are needed. For this, the Mg-Ni alloys are among the most promising candidates since the theoretical discharge capacity of Mg_2Ni (1000 mAh/g) is, for instance, 2.7 times greater than that of $LaNi_5$ (ca. 372 mAh/g) [13–15].

Usually, hydrogen-absorbing alloys are made by melting the different metallic constituents by means of an arc-melting or high-frequency induction furnace. On cooling, the melt solidifies to produce an ingot that is then crushed into fine particles. Such a method, however, presents difficulties when preparing alloys including elements having a high vapor pressure. For instance, because of the high vapor pressure of Mg, the preparation of Mg-based alloys by the melt method was found to be much more difficult than as for the AB_5-type phases. Thus, the need for an alternative synthesis route arose. The mechanical alloying process (MA), involving a solid-state process at ambient temperature, was then tried for producing this type of Mg-based alloys.

Within the field of electrochemically active intermetallic compounds with respect to hydrogen adsorption/desorption, MA is presently enjoying a revival of interest. Recent research groups [15–21] have successfully used this technique to either modify the morphology of the electrode materials, and prepare nanocrystalline alloys or as a coating technique. Kohno et al. [20] have shown that by grinding a mixture of an already made Mg_2Ni alloy and Ni powder in the ratio 1 : 1, they obtained a hydride-forming electrode showing an initial electrochemical capacity of 750 mAh/g of Mg_2Ni, which quickly decreased to less than 500 mAh/g after 10 charge/discharge cycles. Herein, we show that similar electrochemical results can be obtained on Mg-Ni type

alloys directly prepared at room temperature from Mg and Ni powder by mechanical alloying.

Experimental

The starting metallic elements used to perform the MA experiments consisted of elemental Ni powders (having a particle size of 1 μm) prepared in-house by the polyol process (F. Fievet, V. Fievet, F. Lagier, M. Figlarz, private communication) [22]. Magnesium powders of 10 μm particle size were obtained from Aldrich. Mixtures of the desired composition to give 0.5 g of the final alloy were placed into a 12.5-cm^3 internal volume grinding container made of a high-hardness steel (HRC 30) together with one 12-mm diameter stainless steel ball. The sample loading was carried out inside an argon glove box in order to avoid oxygen contamination, and a Viton O-ring was placed on top of the grinding container prior to hermetically sealing with a cover secured by screws. For all the experiments performed, if not otherwise specified, the weight ratio of ball to powder was about 14. The mechanical alloying experiments were performed with a SPEX mixer mill model 8000 under argon atmosphere. This mixer generates impact/shock interactions [23] as the result of the ball hitting the wall of the grinding container.

The characterization of the samples was performed by X-ray diffraction (XRD) with a Philips diffractometer model PW 1710 (Cu K$\alpha = 0.15418$ nm). A numerical method included in the Diffrac-At software was used to analyze the XRD patterns, and to obtain the full width at half height (FWHH) of the diffraction peaks. A decomposition based on the Voigt peak shapes was chosen. The crystallite size was calculated from the Scherrer formula $L(\text{Å}) = 0.94\ \lambda/\beta\cos\theta$, where λ is the X-ray wavelength, β the line width of the sample (in radians) and θ the diffraction angle.

The thermal behavior of the MA samples was investigated by isothermal annealing at 673 K for 5 h under an argon atmosphere using an external furnace. Powders were removed from the furnace after cooling for X-ray characterization.

The morphological study was carried out by scanning electron microscopy with a Philips XL 30 field emission gun (FEG) coupled with an Oxford Link instrument for energy-dispersive X-Ray (EDX) microanalysis. EDX was used to provide, by means of the element mapping facility, information about the powder homogeneity and alloy composition. Finally, all the samples were checked for their oxygen content by means of quantitative chemical analysis.

The electrochemical measurements were realized with an Arbin Battery Test System. We used a three-electrode cell where the negative is a mixture of Mg-Ni alloy and graphite, the positive is a platinum wire, and the reference is an Hg/HgO electrode. The cycling was conducted using the current rate of 100 mA/g hydrogen storage alloy for 10 h, and the discharge was conducted at the current rate of 20 mA/g. The oxidation potential was limited to values lower than −0.5 V. The gravimetric capacity is obtained from the ratio Q/M, where Q is the amount of current of the discharge and M the mass of active material introduced into the electrode.

Results and discussion

Synthesis and characterization of Mg_2Ni and Mg_2Ni_2 alloys

The required amounts of crystalline Mg and Ni powders were mixed in the correct stoichiometry, and milled in an argon atmosphere with a Spex mixer mill model 8000 to obtain the desired Mg-Ni alloys. Mg_2Ni crystallized and Mg_2Ni_2 amorphous alloys were produced after 80-h grinding time as shown by the X-ray diffraction patterns of Fig. 1.

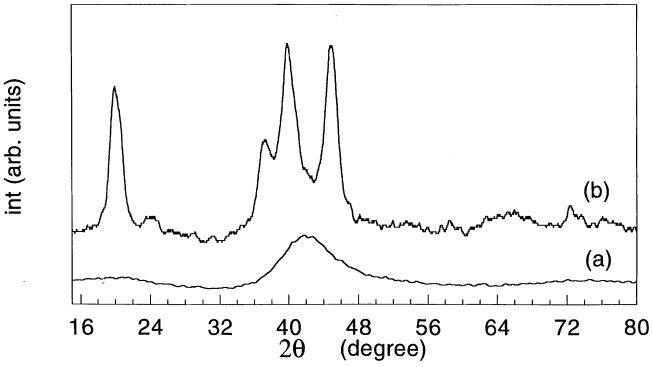

Fig. 1 XRD patterns of Mg-Ni powders obtained after 80 h of grinding time in the Spex mixer mill: **a** Mg_2Ni_2, and **b** Mg_2Ni

The crystallite size evaluated from the broadening of the X ray diffraction lines of the Mg_2Ni alloy is around 70 Å (Table 1), as is usually observed for alloys made by mechanical alloying. Microanalysis measurements performed on MA-made alloys showed that the nominal starting composition was mainly preserved (Table 2). An oxygen contamination of about 0.3% in weight, as determined by chemical analysis, was found for Mg_2Ni and Mg_2Ni_2 alloys. Such an oxygen contamination is most likely linked to the difficulty in producing a perfectly hermetically sealed grinding container. Finally, around 0.2 at% Fe, arising from the interaction between the ball, the powder and the wall of the container, was detected by EDX.

The morphologies of the Mg-Ni alloys as prepared by MA are shown in Fig. 2. The Mg_2Ni_2 particles consist of large agglomerates, with a particle size distribution of 20–100 μm (Fig. 2a). For the Mg_2Ni alloy (Fig. 2b), in contrast, the agglomerates are partially fractured, giving a bimodal particle size distribution; larger particles with

Table 1 Crystallite size L(Å) of the Mg_2Ni alloy in the different [h,k,l]* directions, (a) Mg_2Ni as prepared by MA, (b) Mg_2Ni prepared by MA and followed by a subsequent annealing at 673 K for 5 h under Ar atmosphere

[h,k,l]*	003	101	102	112	105	200	203
a	79	80	51	72	65	63	63
b	900	187	107	169	104	587	587

Table 2 Elemental analyses of Mg_2Ni and Mg_2Ni_2 alloys prepared by MA

Alloy compositions	Mg_2Ni_2	Mg_2Ni
Mg (At%)	49.8	67.7
Ni (At%)	50.0	32.0
Fe (At%)	2.0	1.8
O (At%)	0.3	0.4

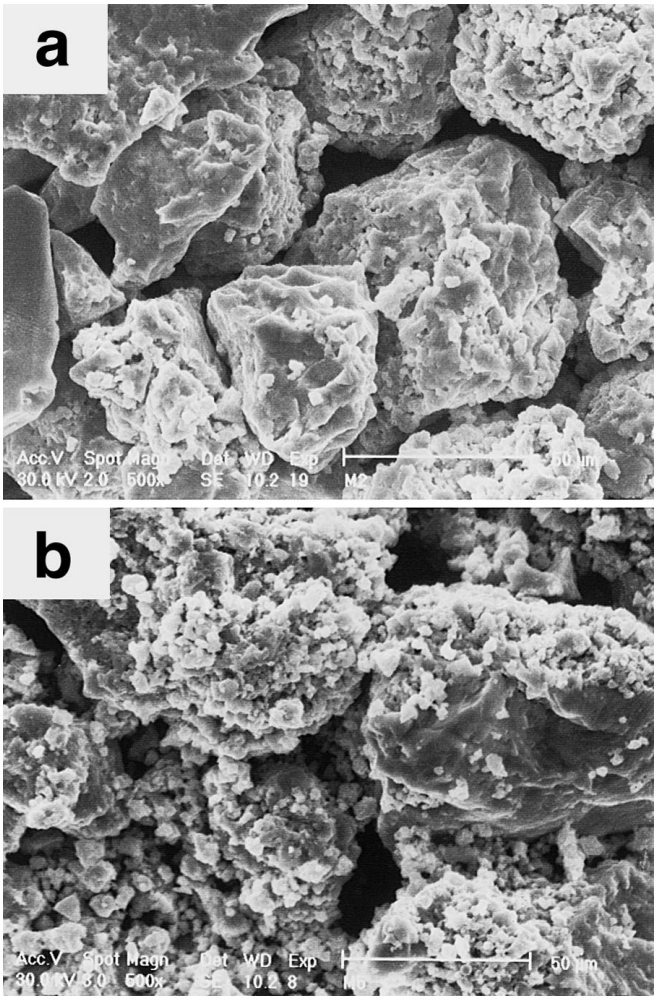

Fig. 2a, b SEM images showing the morphologies of the Mg-Ni powders mixture obtained after 80 h of grinding time in the Spex mixer mill: **a** Mg_2Ni_2, and **b** Mg_2Ni

a size range of 20–100 μm and smaller particles with a size range 1–10 μm.

No Bragg peaks corresponding to metallic nickel could be detected in the X-ray diffraction pattern within the accuracy of the measurements. An investigation for the homogeneity of the Mg_2Ni_2 and Mg_2Ni alloys was done by EDX mapping (Fig. 3). Note a uniform distribution of both alloys, implying that, even in the case of Mg_2Ni_2 (excess of Ni compared to Mg_2Ni), a homogeneous dispersion occurred under mechanical milling. The presence of Ni aggregates could not be found in either part of the samples. Thus, it can be deduced that Mg_2Ni and Mg_2Ni_2 alloys, as prepared by mechanical alloying, are single phases.

Finally, the thermal behavior of these MA-made Mg_2Ni and Mg_2Ni_2 alloys was investigated by isothermal annealing under an argon atmosphere (Fig. 4). We found, as expected on the basis of the binary Mg-Ni phase diagram [24], that at 673 K the metastable Mg_2Ni_2 amorphous alloy transforms into a crystallized mixture of Mg_2Ni and $MgNi_2$, whereas only an increase in the crystallinity is observed for the Mg_2Ni alloy.

Electrochemical behavior of the hydride-forming alloys

Charge/discharge curves for three-electrode cells using different MA-made Mg-Ni alloys are shown in Fig. 5. These curves were obtained on charging at a current rate of 100 mAh/g for 10 h, discharging at a current rate of 20 mA/g until the potential reached −0.5 V, and then, at −0.5 V, discharging in a potentiostatic mode until the current fell to 2 mA/g. The capacity decrease on cycling, for both Mg_2Ni and Mg_2Ni_2 electrodes, is shown in Fig. 6. These results seem to imply that the hydrogen storage properties of Mg-Ni alloys are directly linked to their degree of structural disorder and density of defects (grain boundaries and so on). A simple way to account for this observation is to keep in mind that, as previously reported, mechanical alloying (1) produces alloys with high internal strain and hence numerous defects [25–27], and (2) strongly increases the free energy of the alloy and hence the equilibrium pressure of the hydride-forming material [16, 17, 19]. The usual hydrogenation pressure at 298 K of crystalline Mg-Ni alloys prepared by arc-melting is too low for good electrochemical behavior. So, at the extreme, when an amorphous Mg-Ni is obtained by mechanical alloying, the disorder created in the sample could increase the equilibrium pressure of the hydride until it reaches the range of pressure useful for electrochemical testing leading, thereby, to an increased capacity. This effect can directly be demonstrated by the observation that the electrochemical capacity of crystallized Mg-Ni alloys made by the arc-melting process shows an initial electrochemical capacity of 50 mAh/g [20], while the present alloys, nanocrystalline Mg_2Ni and amorphous Mg_2Ni_2 prepared by mechanical alloying, exhibit initial capacities of 270 mAh/g and 500 mAh/g, respectively. These capacities, however, quickly decrease after only 5 charge/discharge cycles (90 mAh/g and 300 mAh/g), and finally reach 30 mAh/g and 70 mAh/g at 60 cycles.

In an attempt to understand the differences in storage capacities of the Mg_2Ni and Mg_2Ni_2 alloys, namely the rate of capacity decrease that is initially faster for the Mg_2Ni than for the Mg_2Ni_2 alloy, SEM, EDX and XRD analyses have been performed on the alloys after 5 completed charge/discharge cycles. SEM micrographs (Fig. 7) show a drastic surface modification of the particles, as evidenced by the formation of numerous fissures, with the addition of the appearance of well-defined rods, 0.1 μm thick and 0.5 μm long, that turn out to be of $Mg(OH)_2$. The XRD patterns collected for the cycled samples (Fig. 8) reveal important changes with respect to those of the pristine alloys (Fig. 1), the main difference being the appearance of strong extra Bragg peaks corresponding to the formation of $Mg(OH)_2$ upon cycling. The corresponding EDX ele-

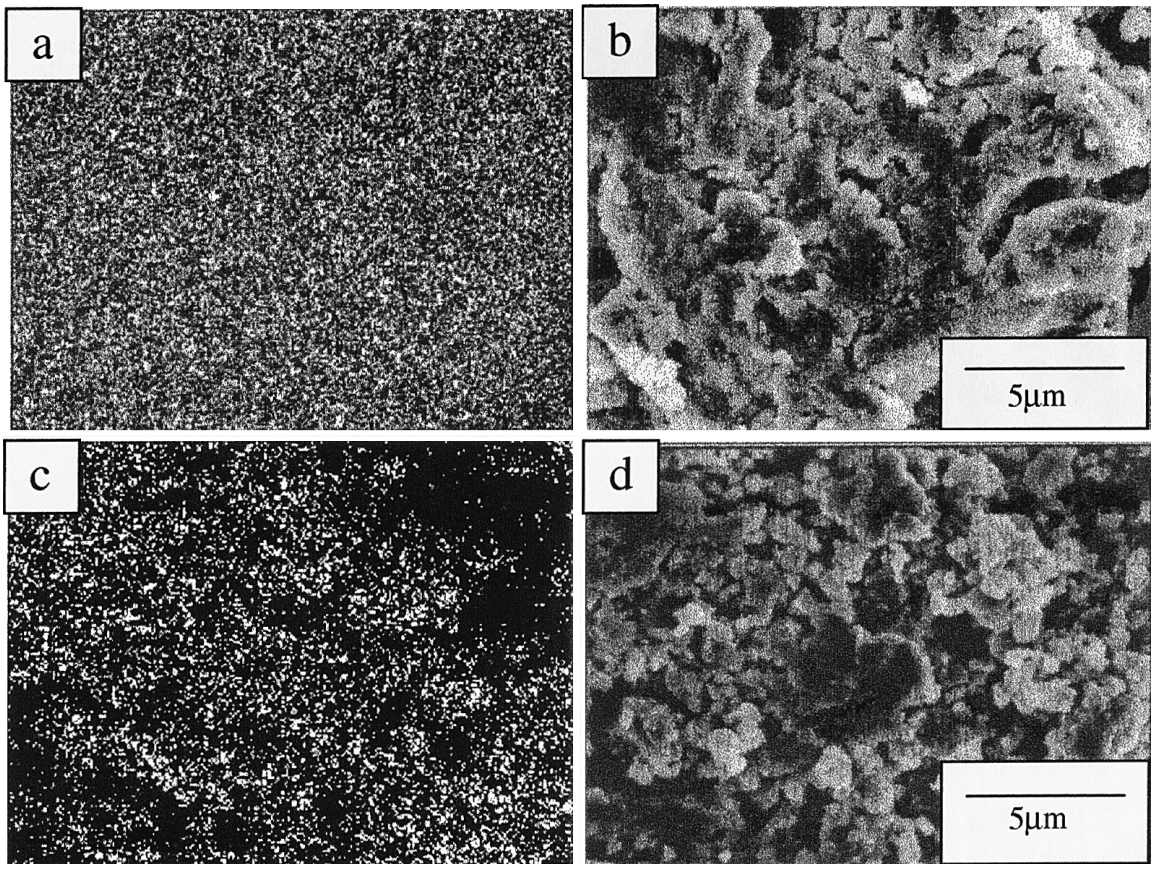

Fig. 3a–d X-ray microanalyses of Mg-Ni alloys obtained after 80 h of milling time: **a** Mg_2Ni_2, and **b** Mg_2Ni

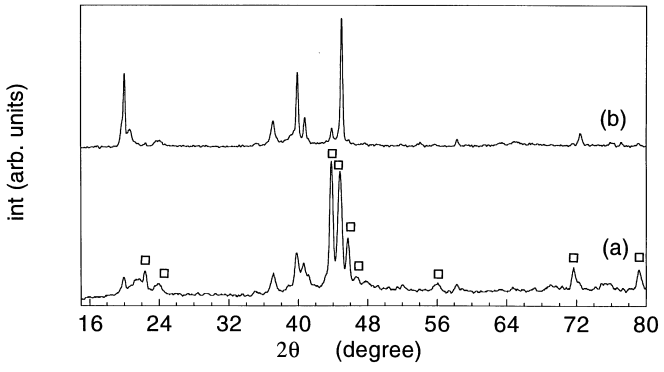

Fig. 4 X-ray diffraction patterns after isothermal annealing at 673 K of **a** Mg_2Ni_2, and **b** Mg_2Ni alloys obtained by mechanical alloying. The main diffraction lines of $MgNi_2$ are indicated by *squares*. Mg_2Ni: *unmarked* diffraction lines

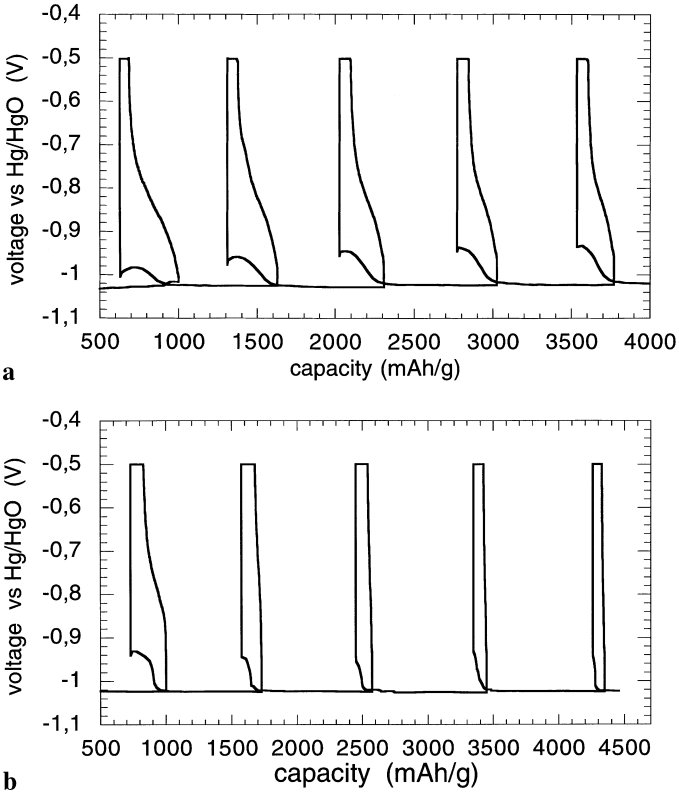

Fig. 5a, b Electrochemical charge/discharge curves for the first 5 cycles of the Mg-Ni alloys prepared by MA after 80 h of grinding time: **a** Mg_2Ni_2, and **b** Mg_2Ni

mental analysis revealed that, after cycling, the surface of the particle is richer in Mg (Table 3) and O than before cycling, supporting the X-ray observations.

Note that this behavior is more pronounced in the case of the Mg_2Ni alloy. Although it is well known that $Mg(OH)_2$ is hardly soluble in KOH media at a pH greater than 9, we could not be sure that there were no

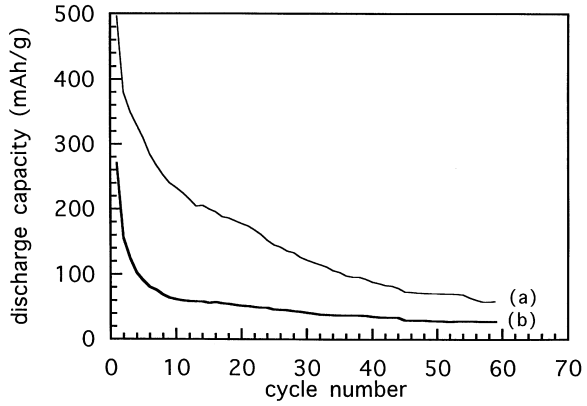

Fig. 6 Discharge capacities as a function of cycle number of Mg-Ni alloys obtained after 80 h of grinding time in the Spex mixer mill by mechanical alloying: **a** Mg_2Ni_2, and **b** Mg_2Ni

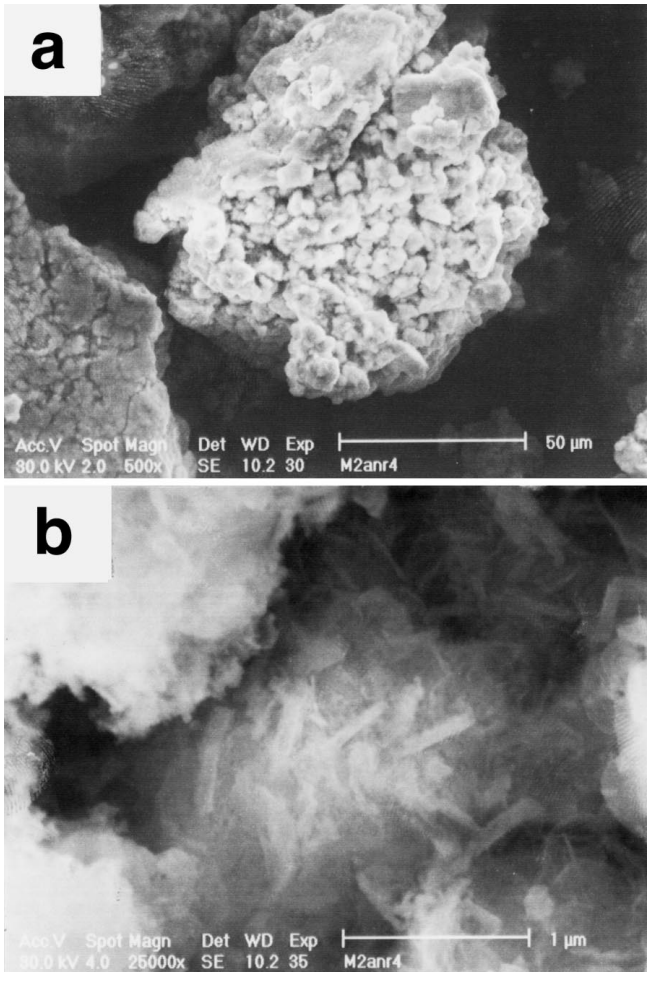

Fig. 7a, b SEM images showing the morphologies of the Mg-Ni alloys after 5 charge/discharge cycles

side reactions that could lead to Mg-based soluble species. This possibility was eliminated by atomic absorption (AA) analysis, which revealed the absence of Mg in our electrolyte (see Table 4).

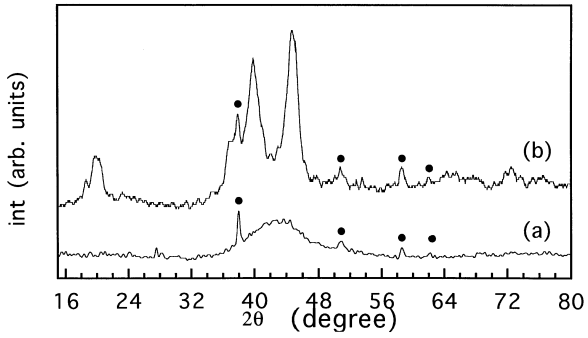

Fig. 8 XRD patterns after 5 charge/discharge cycles of Mg-Ni powders: **a** Mg_2Ni_2, and **b** Mg_2Ni. The main diffraction lines of $Mg(OH)_2$ are marked by *full circles*

Table 3 EDX surface analysis of the Mg-Ni alloys after 5 charge/discharge cycles

Surface composition	Mg_2Ni_2	Mg_2Ni
Mg (At%)	70	78
Ni (At%)	30	22

Table 4 Mg content of KOH electrolyte after 70 charge/discharge cycles

Alloy composition	Mg_2Ni	Mg_2Ni
cycle number	60	60
Mg (mg/g-alloy)	0.6	0.6

The above three findings imply that a strong corrosion of the Mg-Ni alloys occurs during cycling. In the case of the Mg_2Ni_2 alloy, this Mg oxidation is less because of the surface protection by the excess of Ni. The magnesium hydroxide so produced forms a passivation layer on the surface of the hydride-forming alloys, decreasing the electrocatalytic activity for the hydrogen electrode reactions, and preventing hydrogen atoms from being transferred from the surface to the bulk resulting in a strong decrease in the charge efficiency of the material.

Conclusion

We report, to our knowledge for the first time, the feasibility of preparing, at room temperature and in one step from the metallic elements, electrochemically active alloys within the Mg-Ni system by mechanical alloying. However, their large initial capacity was found to decrease rapidly upon cycling, mainly because of the corrosion of Mg during cycling, leading to the formation of $Mg(OH)_2$. Finally, we have shown that Mg_2Ni_2-type alloys obtained by this process had a larger initial capacity and better capacity retention than alloys of the

Mg_2Ni-type. Thus, on this basis, one might expect that an alloy with a higher Ni/Mg ratio will show better resistance against Mg corrosion during cycling. Such a study, presently in progress, will be described in a forthcoming paper.

Acknowledgements The authors thank Y. Chabre and F. Salver-Disma for helpful discussions and J.B. Leriche for technical assistance.

References

1. Sakai T, Muta K, Miyamura H, Kuriyama N, Ishikawa H (1992) In: Corrigan DA, Srinivasan S (eds) Hydrogen storage materials, batteries and electrochemistry. The Electrochemical Society Proceedings Series, PV 92-5. Pennington, NJ, p 59
2. Lynch FE (1991) J Less Common Met 172–174: 943–958
3. Furukawa N (1994) J Power Sources 51: 45–59
4. Ovshinsky SR, Fetcenko MA, Ross J (1993) Science 260: 176
5. Wakao S, Sawa H, Furukawa J (1991) J Less Common Met 172–174, p 1216
6. Moriwaki Y, Gamo Y, Seri H, Iwaki T (1991) J Less Common Met 172–174, p 1216
7. Fetcenko MA, Venkatesan S, Ovshinsky SR (1992) In: Corrigan A, Srinivasan S (eds) Hydrogen storage materials, batteries and electrochemistry, PV 92-5. The Electrochemical Society Proceedings Series, Pennington, NJ, p 141
8. Kim SR, Lee JY (1992) J Alloys Comp 185, L1
9. Züttel A, Meli F, Schlapbach L (1994) J Alloys Comp 203: 235
10. Züttel A, Meli F, Schlapbach L (1994) J Alloys Comp 209: 99
11. Kim SR, Lee JY, Park HH (1994) J Alloys Comp 205: 225
12. D Van Sandrock G, Suda S (1994) J Alloys Comp 216: 237
13. Lupu D, Biris A, Indrea E (1982) Int J Hydrogen Energy 7: 783
14. Reilly JJ, Wiswall RH (1968) Inorg Chem 7: 2254
15. Zaluski L, Zaluska A, Ström-Olsen JO (1995) J Alloys Comp 217: 245
16. Sakaguchi H, Sugioka T, Adachi G (1995) Chem Lett: 561
17. Sakaguchi H, Sugioka T, Adachi G (1996) Eur J Solid State Inorg Chem 33: 101–108
18. Anani A, Visintin A, Petrov K, Srinivasan S (1994) J Power Sources 47: 261–275
19. Lenain C, Aymard L, Disma F, Leriche J-B, Chabre Y, Tarascon JM (1997) J Solid State Ionics 104: 237–248
20. Kohno T, Tsuruta S, Kanda M (1996) ECS Fall Meeting, San Antonio, Texas, October 15
21. Aymard L, Ichitsubo M, Uchida K, Sekreta E, Ikazaki F (1997) J Alloys Comp 259: L5–L7
22. Ducamp-Sanguesa C, Herrera-Urbina R, Figlarz M (1992) J Solid State Chem 100: 272–280
23. Davis RM, McDermott B, Koch CC (1988) Met Trans A, Vol 19A, pp: 2867–2874
24. Nayeb-Hashemi AA, Clark JB (1991) In: Massalski TB (ed) Binary alloy phase diagrams. ASM international edn, p 2529
25. Aymard L, Beaudoin B, Dumont B, Delahaye-Vidal A (1996) J Mater Chem 6: 1537–1541
26. Benghalem A, Morris DG (1994) Acta Metal Mater 42: 4071–4081
27. Aymard L, Delahaye-Vidal A, Portemer F, Disma F (1996) J Alloys Comp 238: 116–127